Determining the energetics of vicinal perovskite oxide surfaces

Werner A. Wessels,[1] Tjeerd R. J. Bollmann,[1,a] Gertjan Koster,[1]
Harold J. W. Zandvliet,[2] and Guus Rijnders[1]
[1]*Faculty of Science and Technology and MESA+ Institute for Nanotechnology, Inorganic Materials Science, University of Twente, P.O. Box 217, 7500 AE Enschede, The Netherlands*
[2]*Faculty of Science and Technology and MESA+ Institute for Nanotechnology, Physics of Interfaces and Nanomaterials, University of Twente, P.O. Box 217, 7500 AE Enschede, The Netherlands*

(Received 17 January 2017; accepted 20 April 2017; published online 1 May 2017)

The energetics of vicinal $SrTiO_3(001)$ and $DyScO_3(110)$, prototypical perovskite vicinal surfaces, has been studied using topographic atomic force microscopy imaging. The kink formation and strain relaxation energies are extracted from a statistical analysis of the step meandering. Both perovskite surfaces have very similar kink formation energies and exhibit a similar triangular step undulation. [http://dx.doi.org/10.1063/1.4982886]

I. INTRODUCTION

The perovskite oxides are a fascinating class of material, due to their wealth in available physical properties, such as superconductivity, ferromagnetism, ferro- and dielectricity. Despite their abundance of functional properties, the ABO_3 perovskite platform shares a common crystal structure with similar lattice parameters. For application within oxide thin film devices, grown multilayer (perovskite) heterostructures typically contain at least one functional active layer which is then directly supported onto a substrate, or with a bottom electrode layer in between film and substrate. In these (ultra)thin film structures enormous strains might be beneficial, as they can result in unanticipated functional properties such as altering T_c of ferromagnetic and superconducting materials.[1–4] However, uncontrolled strain relaxation might also result in destructive cracking[5–7] or threading dislocation cascades[8–10] within thin films. It is therefore of utmost importance to identify and quantify strain relaxation behavior within (ultra)thin films. As we will demonstrate furtheron, strain relaxation phenomena are easily identified at the thin film interface. Besides strain relaxation, the kink formation energy is an important parameter in thin film growth, facilitating nucleation during growth and thereby determining the resulting growth to be either of rough 3D or 2D stepflow character. The formation of steps usually introduces surface stress, influencing the step edge morphology. In view of its technological relevance, most of the step-related surface studies have been focused so far on silicon as a model system.[11,12]

In this paper, we describe a method to determine both, the strain relaxation energy together with the step edge formation energy by the use of Atomic Force Microscopy (AFM) as it can image the surface topography irrespective of its band gap. To our knowledge, this study is unique in the field of complex oxides as it is a quantitative study to extract energetic parameters using AFM where AFM studies reported in literature so far[13–15] have been of qualitative character. By imaging the meandering of step edges, which are determined by the step free energy, the kink formation energy can be determined.[16] As in mono-metal oxides the geometric structure at the surface is considered to be a continuation of the atomic arrangement of building blocks,[17] we assume in our analysis that for

[a]Corresponding author: t.r.j.bollmann@utwente.nl.

the more complex perovskite oxides the ABO_3 building block is the elementary unit to describe the surface energetics.

This paper is arranged as follows. First, we describe the experimental details with emphasis on the surface preparation to ensure the surface under study is in thermal equilibrium. Next, we explain the use of correlation functions to extract the kink energy (E_{kink}) and strain relaxation energy constant (C) from the observed step meandering in topographical AFM images. Finally, we discuss the use of this procedure on two prototypical perovskite surfaces, i.e. $SrTiO_3(001)$ and $DyScO_3(110)$. We conclude by summarizing the observed findings and argue how the reported implications are anticipated to be of generic character.

II. EXPERIMENTAL DETAILS

To quantify the strain relaxation energy, we image the step meandering of vicinal perovskite surfaces on standard commercial available 5×5 mm^2 samples of $SrTiO_3(001)$ and $DyScO_3(110)$ using topographical AFM images. $SrTiO_3(001)$ and $DyScO_3(110)$ samples are often used substrates in thin film growth studies, as they are chemically stable and are known to have a low defect density. In addition, these materials have a well-defined surface of alternating AO and BO_2 planes, which is neutral in the case of $SrTiO_3(001)$ and polar for $DyScO_3(110)$. Furthermore, $SrTiO_3(001)$ has a cubic lattice constant of a_0=3.905Å whereas $DyScO_3(110)$ has a nearly square surface mesh with an inplane lattice spacing of a_0=3.95Å in the perovskite oxide spectrum.[18] The assumption of a cubic unit cell for both was used throughout our analysis. Note that therefore the step formation energy for the described isotropic square surface lattice equals the kink energy.

Prior to annealing, all samples were ultrasonically rinsed in acetone and ethanol both for 10 minutes. In order to achieve single terminated BO_2 surfaces, we applied chemical etching procedures as described in detail elsewhere.[19,20] The samples were then annealed in a tube furnace using an O_2 flow of 150 l/h at a temperature of 1273 K. The AFM topographic images were taken in *ex-situ* tapping mode (TM). The fast scan direction was aligned perpendicular to the surface steps in order to optimize image analysis and to prevent tip artifacts in the images.

For the statistical analysis described below, it is of utmost importance that the surface is prepared at thermal equilibrium. By varying the annealing time and temperature followed by AFM imaging, we study the evolution of the step-edges to find the conditions for which the surface is at equilibrium. Fig. 1(a) shows the polished as-received surface, exhibiting disordered step edges, without a well-defined step distribution. Upon 30 minutes of annealing as described above, the steps become visible, but still reveal vacancy islands in the terraces as well as protrusions along the step edges, indicative of its non-equilibrium state, see Fig. 1(b). Prolonged annealing up to 4 hours results in meandering of the surface steps and a well-defined and narrow terrace width distribution, see Fig. 1(c) and (f). The average terrace width measured, is found to slightly vary over the sample, within 20%. No vacancy islands are present in the terraces. In order to verify the persistence of the single terminated BO_2 surfaces upon several hours of annealing, we checked the phase-lag images corresponding to the topographic images shown in Fig. 1, see Fig. S1 of the supplementary material. In line with the observations in Ref. 15, and Fig. 4(a) and (b) therein, no segregation was observed upon increased annealing time. Typically, the average terrace width ($< L >$) and its standard deviation (σ) are measured to study the strength of the step-step interactions. To verify the terrace width, its distribution P(l) versus the terrace width l is plotted in Fig. 1(f). The data can nicely be described by the fitted Gaussian, neglecting the weak shoulders and the slight asymmetry in the distribution. An average terrace width $< L >$ of 760 a_0 (corresponding to 300 nm) is found for the $DyScO_3(110)$ surface in Fig. 1(c). The standard deviation (σ) of this distribution, only 86 a_0 (corresponding to 34 nm), is small with respect to $< L >$ and indicative for step-step interactions. This very narrow distribution of $DyScO_3(110)$ compared to silicon can be explained by the coherent behavior of the $DyScO_3(110)$ step-edges.[11]

Continuing annealing up to 12 hours, see Fig. 1(d), reveals no significant change of the surface or step edge correlation function analysis as described below, a clear signature of a surface at thermal equilibrium. The same procedure was used to prepare and verify the $SrTiO_3(001)$ surface at thermal equilibrium, see Fig. 1(e). Note that the time at which thermal equilibrium is reached scales as t^{α}, where t is the time and α an exponent that depends on the exact mass transport mechanism.[21–23] An

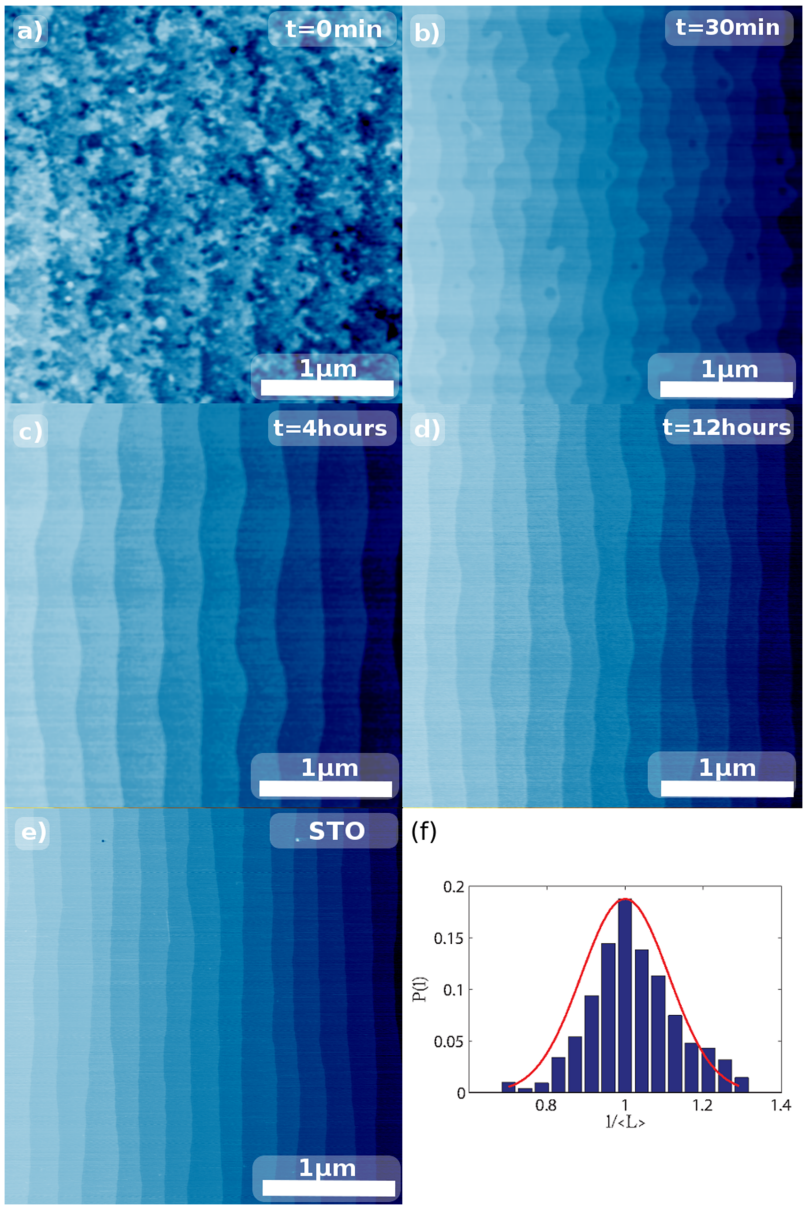

FIG. 1. *Ex-situ* TM-AFM images of $DyScO_3$(110) surface at room temperature of a) an as-received surface, b) surface after 30 min annealing at 1273 K, c) surface after 4 hours annealing at 1273 K and d) surface after 12 hours annealing at 1273 K, respectively. Note that these samples were cut from the same crystal. e) *Ex-situ* TM-AFM image of $SrTiO_3$(001) surface at thermodynamic equilibrium. $< L >$=250 nm, σ=37 nm. f) Normalized terrace width distribution P(l) vs. terrace width l of the $DyScO_3$(110) surface annealed for 4 hours at 1273 K. An average terrace width $< L >$ = 300 nm is found. The narrow width σ = 34 nm and asymmetry are indicative for entropic and energetic step-step interactions.

exponent $\alpha = \frac{1}{2}$ describes mass exchange between the step edge and adatoms on the terrace, whereas $\alpha = \frac{1}{4}$ describes mass transport along step edges.[24] The large correlation length determined from the experimental obtained data ($\lambda \approx 2100\ a_0$, see below) suggests that a non-equilibrium step instability is very unlikely.[25,26]

III. STATISTICAL ANALYSIS

In order to extract the kink energy E_{kink} and strain relaxation energy from the meandering step edges in the topographical AFM images, step edge analysis was performed on the AFM images by

first applying a Gaussian filter to reduce noise. Subsequently, leveling of the height data was done by plane fitting the topography. Step edges were then detected by applying the Canny filter,[27] a multi-stage algorithm to detect a wide range of edges. Fig. 2(a) represents a processed AFM topographical image of a $DyScO_3(110)$ at thermal equilibrium after 4 hours of annealing. The lines in Fig. 2(a) represent the step edges, detected by the Canny filter.

The step meandering of perovskite oxide step edges can be represented by a triangular undulation as can be seen from the triangular nature of the undulations in the experimentally obtained AFM data, see e.g. Fig. 1(e). The triangular undulation can be described by amplitude A and wavelength λ as schematically shown in Fig. 2(b). The continuous wavy line labeled by w is representing the step meandering of the step edge, corresponding to the white lines in Fig. 2(a) representing the $DyScO_3(110)$ step edges in this example. The mean line of the meandering of the step edge is represented by m.

Now, by measuring the deviation-deviation correlation function $G(r)$ of the step one can extract the mean square kink length:[11]

$$G(r) = < (h(r) - h(0))^2 > = < k^2 > \frac{r}{a_0} \tag{1}$$

where $h(r)$ is the deviation measured in the direction perpendicular to the step edge at position r, $h(0) = < h(r) > = 0$ is the deviation measured in the direction perpendicular to the step edge at position 0, r is the position along the high symmetry direction parallel to the step edge, and a_0 the unit cell length parallel to the step edge. Now $< k^2 >$ is the mean-square kink length. From the mean square kink length, the kink energy can be calculated as:[11]

$$< k^2 > = \frac{\sum_{k=-\infty}^{\infty} k^2 e^{\frac{-E_{kink}(k)}{k_B T}}}{\sum_{k=-\infty}^{\infty} e^{\frac{-E_{kink}(k)}{k_B T}}} \tag{2}$$

where k is the kink length, k_B the Boltzmann constant and T the sample temperature. The kink energy for a kink with length $k \cdot a_0$ is related to the nearest neighbour energy E_{nn} as:

$$E_{kink}(k) = k \cdot E_{nn}/2 \tag{3}$$

From here on $E_{kink}(1)$ is referred to as E_{kink}. By substitution, the mean square kink length $< k^2 >$ and kink energy E_{kink} relation can be simplified to (see supplementary material):

$$< k^2 > = \frac{2y}{(1-y)^2} \tag{4}$$

where:

$$y = e^{\frac{-E_{kink}}{k_B T}} = e^{\frac{-E_{nn}}{2k_B T}} \tag{5}$$

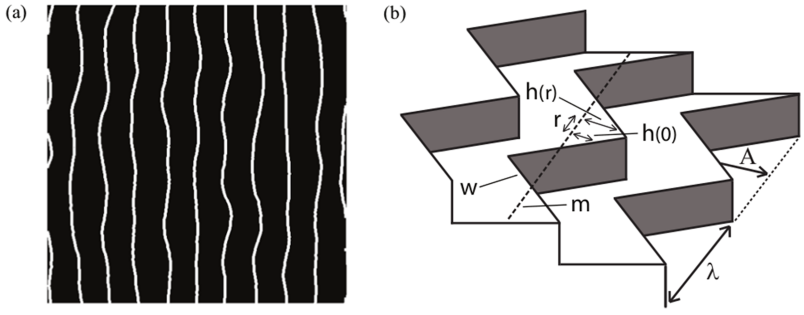

FIG. 2. Statistical analysis on a 512×512 pixels^2 *ex-situ* TM-AFM image. a) The Canny method applied to an AFM image of $DyScO_3(110)$ to obtain the step edge profiles (displayed here in white). b) Schematic representation of a triangular step edge undulation amplitude A and wavelength λ. The wavy w line represents a step edge of the surface whereas its mean line is indicated by m.

Eqs. 1–5 reveal that the kink energy E_{kink} can be extracted by measuring the slope $< k^2 >$ of the correlation function for small enough r.[11,28] The linear dependence in this range of the correlation function implies a random kink formation distribution.

In order to determine the strain energy, we fit the correlation function of the perovskite oxide step waviness by a triangular step undulation model. Note that the triangular step undulation is indicative of a strong energy relaxation mechanism along the step. There is a competition between two energy terms in minimizing the surface free energy, i.e. the energy cost to create additional step length versus the energy reduction by strain relaxation due to the triangular undulations along the step edge.

The total free energy per unit area F of a triangular step edge, see also supplementary material Eq. S12 and onward,[29] is equal to:

$$F = \gamma + \frac{2F_{step}}{\lambda} - \frac{2C}{\lambda} ln(\frac{\lambda}{2\pi a}) + \frac{2Cln(2)}{\lambda} \tag{6}$$

where γ is the free energy per unit area (in perovskite oxides, the free energy per unit area for a step-up and step-down domain are equal) and F_{step} is the step free energy per unit length. The strain relaxation energy constant C is defined in Eq. S14, see also supplementary material. The critical periodicity λ_c follows from the minimum free energy per unit area by calculating $\frac{dF}{d\lambda}$=0 as:

$$\lambda_c = 2\pi a e^{(\frac{F_{step}}{C} + 1 + ln(2))} \tag{7}$$

Besides the ln(2) term in the exponent, Eq. 7 is identical to the relation derived by Alerhand *et al.*[28] Note that for other models, such as a sinusoidal or a block wave, the results are in essence similar, albeit with a slightly different prefactor.

Now, by determining the critical periodicity λ_c from the experimentally obtained topographic AFM images, together with the obtained E_{kink} (extracted from the slope $< k^2 >$ of the correlation function for small enough r), one can calculate the strain relaxation energy constant C.

IV. ENERGETICS OF $SRTIO_3$(001) AND $DYSCO_3$(110) SURFACES

In order to demonstrate how the energetics of vicinal perovskite surfaces can be studied by measuring its surface topography, we determine the E_{kink} and strain relaxation for two prototypical perovskites i.e. $SrTiO_3$(001) and $DyScO_3$(110). For this, we performed the image analysis as described on Fig. 1(e) and (c) respectively, identifying the step edges by use of the described Canny filter. From these, we calculated the corresponding (average) correlation functions as depicted in Fig. 3 which show surprisingly both qualitative and quantitave similarities for $SrTiO_3$(001) and $DyScO_3$(110). In Fig. 3(a), the average correlation functions are shown for $SrTiO_3$(001) and $DyScO_3$(110) step edges with in the inset the correlation function of a single step edge. At large length scales, see Fig. 3(a), the correlation functions of both systems show a clear correlation with an average periodicity λ, which slightly varies from step to step. Multiple minima and maxima are present demonstrating the strong correlation along the step edges. The ratio between minima and maxima of the triangular undulation with amplitude A, see Fig. 2(b), slightly varies from step to step, however, the periodicity remains constant for both material systems.

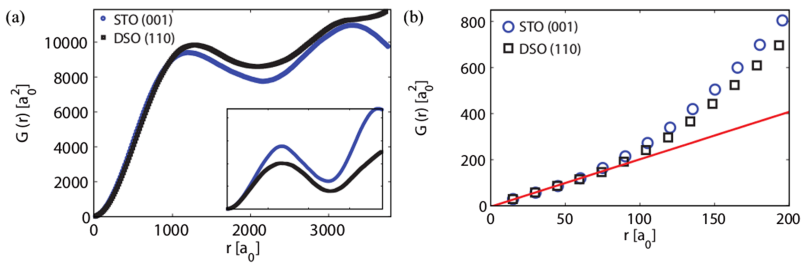

FIG. 3. Average correlation functions of $SrTiO_3$(001) (STO) and $DyScO_3$(110) (DSO) surface step edges (a). The inset shows a correlation function of a single step edge. The correlation functions show an average periodicity of $\lambda \approx 2100\ a_0 \approx 830$ nm for both surfaces, with only small variations from step edge to step edge. (b) The same correlation function for small r (r=0 - 200 a_0). The average terrace widths, $< L >$, are in the range of 250 - 300 nm having σ in the range of 34 - 37 nm.

In Fig. 3(b), the correlation functions are plotted for small r ranging from 0 - 200 a_0. At short length scales, see Fig. 3(b), the correlation function starts to deviate from the linear fit ($G(r) \sim r$) around $r > 60\ a_0$ to a quadratic relation ($G(r) \sim r^2$).

From the determined correlation function, the critical periodicity λ_c for both surfaces is found to be equal to 2100 a_0 (corresponding to $\approx$ 830 nm). Applying this to Eq. 7 results in a ratio of $\frac{F_{step}}{C} = \frac{E_{kink}}{C} = 4.13$. Now, the kink formation energy can be determined from Fig. 3(b), a $< k^2 > = 2.1 \pm 0.1 a_0^2$ is extracted assuming random kink formation on this short length scale, which results in $E_{kink} = 0.10$ eV/a_0 using Eqs. 4 and 5. Note, that from the nearest neighbour energy E_{nn} can be determined as $E_{nn} = 0.21 \pm 0.01$ eV for $SrTiO_3$(001) and $DyScO_3$(110), both assumed as a (pseudo-)cubic crystal structure.[30] Furthermore, the strain relaxation energy constant C, see also Eq. S14, can then be determined as 24 meV/a_0 for both surfaces. This value is close to the reported value range of $E_{nn} = 0.25$ - 0.6 eV, commonly used in Kinetic Monte Carlo simulations to simulate thin film growth.[31]

As mentioned before, the correlation along the surface steps depends on the average terrace width $< L >$. When the average terrace width becomes too small, the correlation function becomes less pronounced resulting in overestimating E_{kink}. A small terrace width distribution as demonstrated for $DyScO_3$(110) is indicative of step-step interactions. However, in the case that step-step interactions are present, the step-edge morphology, correlation function and extracted energetic values

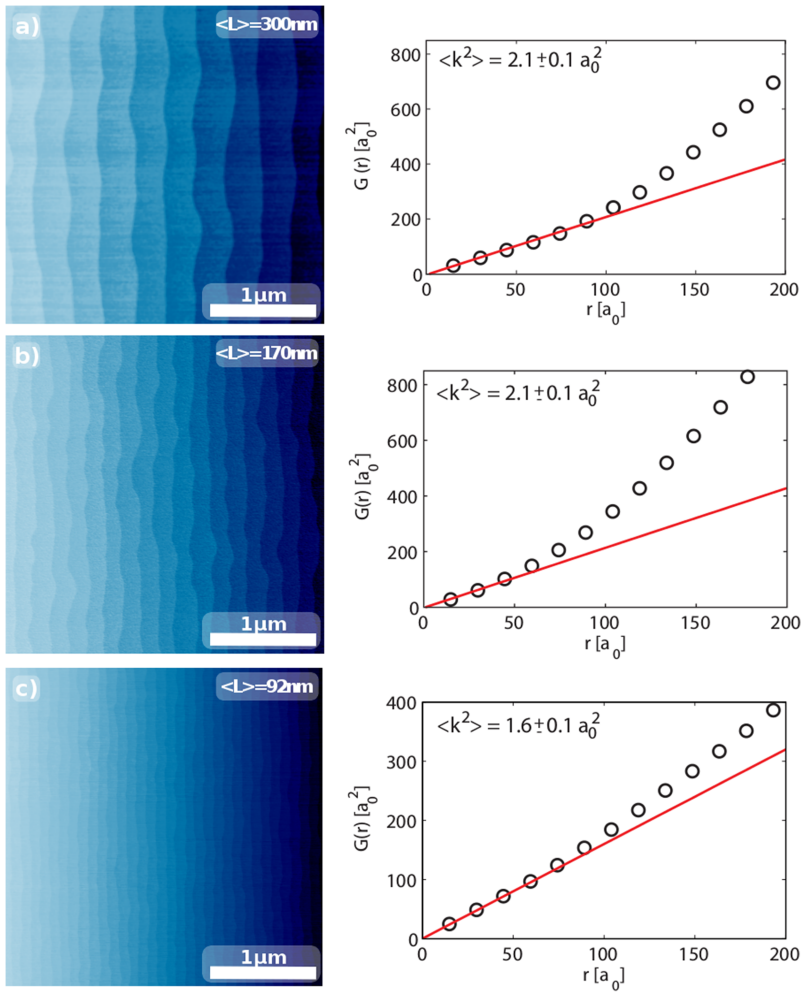

FIG. 4. *Ex-situ* TM-AFM images of annealed $DyScO_3$(110) with different vicinal angles in the left panel labeled with their average terrace width. In the right panel the accompanying average correlation functions are plot with indicated mean square kink length.

can be influenced when terrace widths become so small that step edges start interacting. In Fig. 4 we demonstrate this, by studying $DyScO_3(110)$ samples with increasing vicinal cut. For an average terrace width of only $< L >$=92 nm, the step edge morphology is influenced, resulting in a skewed correlation function which in its turn results to an overestimated nearest neighbour energy.

For larger terrace widths of 300 nm and 170 nm, see respectively Fig. 4(a) and (b), a similar correlation function behavior is found on small length scales (0 - 100 a_0). At larger length scales (1000 - 3000 a_0) the correlation has less pronounced minima and maxima than for the $DyScO_3(110)$ surface having smaller terrace widths ($< L >$ = 170 nm). The mean square kink length is then influenced by the step-step repulsion, which results from entropic reasons and the minimization of surface free energy.[11] For increasing step-step repulsion, the mean square kink length decreases, as the entropy of steps decreases for small step-step separations. Typically, the influence of the step-step interaction potential on a wandering step increases with $\frac{1}{L^2}$.[11] The decrease of the mean square kink length $< k^2 >$ = 2.1 ± 0.1 a_0^2 towards lower values (we described $< k^2 >$ = 1.6 ± 0.1 a_0^2 for $< L >$=92 nm here) results in a change of the found nearest neighbour energy of E_{nn} = 0.21 ± 0.01 eV towards 0.23 ± 0.01 eV. Note that for increasing azimuthal step orientation, the step-free energy per unit length only marginally increases.[32]

The proposed model explains the quasi 1D character of a perovskite oxide step edge for terrace widths larger than 170 nm as the influence of the step-step repulsion can be neglected. Smaller terrace widths show a more 2D character caused by the step-step interaction, which requires a more sophisticated model. Both, the entropic step-step interaction[33] and step interaction energy models[28] used to describe the interaction of Si step-edges are not valid for $DyScO_3(110)$ step-edges. The models assume a meandering Si step-edge catched between two straight step-edges, while the triangular undulation of step-edges on a $DyScO_3(110)$ surface behaves coherent.

V. CONCLUSIONS

In conclusion, we demonstrated a method to determine both, the strain relaxation energy together with the step edge formation energy on a perovskite surface by measuring its vicinal surface topography by use of AFM. Remarkably, we find similar triangular step edge undulations for two different perovskite surfaces at thermal equilibrium. From these we determine an average step edge undulation periodicity of ≈ 2100 a_0 for the two different perovskite materials i.e. $SrTiO_3(001)$ and $DyScO_3(110)$. These step undulations are caused by strain relaxation along the step direction, determined to be 24meV/a_0. From the slope of the correlation function we determine also similar kink formation energies for both perovskite materials to be 0.10 eV/a_0 and corresponding nearest neighbour energy of 0.21±0.01 eV, in good agreement with values used in Kinetic Monte Carlo simulations of thin film growth.[31]

SUPPLEMENTARY MATERIAL

See supplementary material for the supporting AFM phase-lag images corresponding to the topographic images shown in Fig. 1 and the derivation of Eq. 4 and 6.

ACKNOWLEDGMENTS

This work is part of the research programme of NanoNext NL and of the Foundation for Fundamental Research on Matter (FOM), which is financially supported by the Netherlands Organization for Scientific Research (NWO).

[1] R. S. Beach, J. A. Borchers, A. Matheny, R. W. Erwin, M. B. Salamon, B. Everitt, K. Pettit, J. J. Rhyne, and C. P. Flynn, "Enhanced curie temperatures and magnetoelastic domains in Dy/Lu superlattices and films," Phys. Rev. Lett. **70**, 3502–3505 (1993).

[2] H. Sato and M. Naito, "Increase in the superconducting transition temperature by anisotropic strain effect in (001) $La_{1.85}Sr_{0.15}CuO_4$ thin films on lasralo$_4$ substrates," Physica C: Superconductivity **274**, 221–226 (1997).

[3] Q. Gan, R. A. Rao, C. B. Eom, J. L. Garrett, and M. Lee, "Direct measurement of strain effects on magnetic and electrical properties of epitaxial $SrRuO_3$ thin films," Applied Physics Letters **72**, 978–980 (1998).

[4] I. Bozovic, G. Logvenov, I. Belca, B. Narimbetov, and I. Sveklo, "Epitaxial strain and superconductivity in $La_{2-x}Sr_xCuO_4$ thin films," Phys. Rev. Lett. **89**, 107001 (2002).
[5] J. Beuth, "Cracking of thin bonded films in residual tension," International Journal of Solids and Structures **29**, 1657–1675 (1992).
[6] Z. Xia and J. W. Hutchinson, "Crack patterns in thin films," Journal of the Mechanics and Physics of Solids **48**, 1107–1131 (2000).
[7] K. Morito and T. Suzuki, "Effect of internal residual stress on the dielectric properties and microstructure of sputter-deposited polycrystalline (Ba,Sr)TiO_3 thin films," Journal of Applied Physics **97**, 104107 (2005).
[8] F. Ernst, A. Recnik, P. Langjahr, P. Nellist, and M. Rhle, "Atomistic structure of misfit dislocations in $SrZrO_3$/$SrTiO_3$ interfaces," Acta Materialia **47**, 183–198 (1998).
[9] S. H. Oh and C. G. Park, "Misfit strain relaxation by dislocations in $SrRuO_3$/$SrTiO_3$ (001) heteroepitaxy," Journal of Applied Physics **95**, 4691–4704 (2004).
[10] Y. Wang, S. G. Kim, and I.-W. Chen, "Control of strain relaxation in tensile and compressive oxide thin films," Acta Materialia **56**, 5312–5321 (2008).
[11] H. J. W. Zandvliet, "Energetics of Si(001)," Reviews of Modern Physics **72**, 593–602 (2000).
[12] N. C. Bartelt, J. L. Goldberg, T. L. Einstein, and E. D. Williams, "The equilibration of terrace width distributions on stepped surfaces," Surface Science **273**, 252–260 (1992).
[13] T. Nishimura, A. Ikeda, H. Namba, T. Morishita, and Y. Kido, "Structure change of TiO_2-terminated $SrTiO_3$(001) surfaces by annealing in O_2 atmosphere and ultrahigh vacuum," Surface Science **421**, 273–278 (1999).
[14] J. G. Connell, B. J. Isaac, G. B. Ekanayake, D. R. Strachan, and S. S. A. Seo, "Preparation of atomically flat $SrTiO_3$ surfaces using a deionized-water leaching and thermal annealing procedure," Applied Physics Letters **101**, 251607 (2012).
[15] F. Sanchez, C. Ocal, and J. Fontcuberta, "Tailored surfaces of perovskite oxide substrates for conducted growth of thin films," Chemical Society Reviews **43**, 2272–2285 (2014).
[16] H. J. W. Zandvliet, B. Poelsema, and H. B. Elswijk, "Fluctuations of monatomic steps on Si(001)," Phys. Rev. B **51**, 5465–5468 (1995).
[17] V. E. Henrich and P. A. Cox, *The Surface Science of Metal Oxides* (Cambridge University Press, 1996).
[18] D. G. Schlom, L. Q. Chen, X. Pan, A. Schmehl, and M. A. Zurbuchen, "A thin film approach to engineering functionality into oxides," Journal of the American Ceramic Society **91**, 2429–2454 (2008).
[19] G. Koster, B. L. Kropman, G. J. H. M. Rijnders, D. H. A. Blank, and H. Rogalla, "Quasi-ideal strontium titanate crystal surfaces through formation of strontium hydroxide," Applied Physics Letters **73**, 2920 (1998).
[20] J. E. Kleibeuker, G. Koster, W. Siemons, D. Dubbink, B. Kuiper, J. L. Blok, C. H. Yang, J. Ravichandran, R. Ramesh, J. E. ten Elshof, D. H. A. Blank, and G. Rijnders, "Atomically defined rare-earth scandate crystal surfaces," Advanced Functional Materials **20**, 3490 (2010).
[21] W. W. Mullins, "Theory of thermal grooving," Journal of Applied Physics **28**, 333–339 (1957).
[22] W. W. Mullins, "Flattening of a nearly plane solid surface due to capillarity," Journal of Applied Physics **30**, 77–83 (1959).
[23] W. W. Mullins, in *Metal Surfaces: Structure, Energetics and Kinetics* (Am. Soc. Metals, Metals Park, OH, USA, 1963), p. 17.
[24] A. Pimpinelli, J. Villain, D. E. Wolf, J. J. Métois, J. Heyraud, I. Elkinani, and G. Uimin, "Equilibrium step dynamics on vicinal surfaces," Surface Science **295**, 143–153 (1993).
[25] F. Wu, S. G. Jaloviar, D. E. Savage, and M. G. Lagally, "Roughening of steps during homoepitaxial growth on Si(001)," Phys. Rev. Lett. **71**, 4190–4193 (1993).
[26] G. S. Bales and A. Zangwill, "Morphological instability of a terrace edge during step-flow growth," Phys. Rev. B **41**, 5500–5508 (1990).
[27] J. Canny, "A computational approach to edge detection," Pattern Analysis and Machine Intelligence **8**, 679–698 (1986).
[28] O. L. Alerhand, D. Vanderbilt, R. D. Meade, and J. D. Joannopoulos, "Spontaneous formation of stress domains on crystal surfaces," Phys. Rev. Lett. **61**, 1973–1976 (1988).
[29] H. J. W. Zandvliet, "The Ge(001) surface," Physics Reports **388**, 1–40 (2003).
[30] H. J. W. Zandvliet, H. B. Elswijk, E. J. Loenen, and D. Dijkkamp, "Equilibrium structure of monatomic steps on vicinal Si(001)," Phys. Rev. B **45**, 5965 (1992).
[31] P. M. Lam, S. J. Liu, and C. H. Woo, "Monte Carlo simulation of pulsed laser deposition," Phys. Rev. B **66**, 045408 (2002).
[32] H. J. Zandvliet, "Step free energy of an arbitrarily oriented step on a rectangular lattice with nearest-neighbor interactions," Surface Science **639**, L1–L4 (2015).
[33] E. E. Gruber and W. W. Mullins, "On the theory of anisotropy of crystalline surface tension," Journal of Physics and Chemistry of Solids **28**, 875–887 (1967).